# Redox-Switching in a Viologen-type Adlayer: An Electrochemical Shell-Isolated Nanoparticle Enhanced Raman Spectroscopy Study on Au(111)-(1×1) Single Crystal Electrodes

**Bo Liu,[†,⊥] Alfred Blaszczyk,[‡,§] Marcel Mayor,[‡] and Thomas Wandlowski[†,*]**

[†]Departement of Chemistry and Biochemistry, Bern University, Freiestrasse 3, 3012 Bern, Switzerland and [‡]Departement of Chemistry, University of Basel, St.-Johanns-Ring 19, 4056 Basel, Switzerland, and Karlsuhe Institute of Technlogy (KIT), Institute for Nanotechnology, P.O. Box 3640, 76021 Karlsruhe, Germany. [§]Present address: Poznan University of Economics, Department of Commodity Science, Al. Niepodleglosci 10, 61−875 Poznan, Poland. [⊥]Present address: Department of Chemistry, College of Chemistry and Chemical Engineering, Xiamen University, Xiamen 361005, China

**ABSTRACT** We reported the first application of *in situ* shell-isolated nanoparticle enhanced Raman spectroscopy (SHINERS) to an interfacial redox reaction under electrochemical conditions. We construct gap-mode sandwich structures composed of a thiol-terminated HS-6V6H viologen adlayer immobilized on a single crystal Au(111)-(1×1) electrode and covered by Au(60 nm)@$SiO_2$ core−shell nanoparticles acting as plasmonic antennas. We observed high-quality, potential-dependent Raman spectra of the three viologen species $V^{2+}$, $V^{+\bullet}$, and $V^0$ on a well-defined Au(111) substrate surface and could map their potential-dependent evolution. Comparison with experiments on powder samples revealed an enhancement factor of the nonresonant Raman modes of ~$3 \times 10^5$, and up to $9 \times 10^7$ for the resonance modes. The study illustrates the unique capability of SHINERS and its potential in the entire field of electrochemical surface science to explore structures and reaction pathways on well-defined substrate surfaces, such as single crystals, for molecular, (electro-)-catalytic, bioelectrochemical systems up to fundamental double layer studies at electrified solid/liquid interfaces.

**KEYWORDS:** SHINERS · surface-enhanced Raman spectroscopy · core−shell nanoparticles · viologen · single crystal surfaces · electrochemistry

Surface-enhanced Raman scattering is a powerful spectroscopic technique to study molecular adsorption and reaction mechanisms at metal | electrolyte interfaces.[1−3] The application of the method was initially limited to rough or "nanostructured" surfaces of "free-electron-like" metals, that is, Au, Ag, and Cu, and subsequently extended toward transition metals by exploiting various concepts of "borrowing" SERS activity.[4,5] The enhancement of Raman scattering has been attributed to two principle mechanisms, an electromagnetic and/or a chemical ("charge-transfer") enhancement.[6,7] The fast development in nanotechnology during the last 10 years led to a wide range of template and nanoparticle-based fabrication strategies of novel SERS-active plasmonic nanostructures of controlled size, shape, and composition to approach single molecule sensitivity and specificity, and to overcome the problem of ill-defined surface morphology of roughened samples.[7] Examples for applications at electrochemical solid | liquid interfaces are gold and silver nanoclusters,[8−10] nanorods,[11] Pt-group metal-coated Au core−shell nanoparticles[4,12] or templates based on anodic aluminum oxide films[13] and nanosphere lithography.[14−16]

However, the extension of the SERS technique to well-defined single crystal metal|electrolyte interfaces, which is indispensible for a detailed characterization of structure−property relationships, remained a major challenge. The first Raman spectra were reported by Otto *et al.*[17] These authors studied the potential-dependent adsorption of sulfate ions and water molecules from aqueous electrolyte on a vicinal Cu(110) surface employing an attenuated total reflection (ATR) configuration. Attempts to apply tip-enhanced Raman spectroscopy (TERS), a method with high spatial and chemical resolution on single crystal surfaces,[18−20] to electrochemical conditions, were not yet successful.[21] However, recently Ikeda *et al.* showed that high-quality Raman spectra of

* Address correspondence to thomas.wandlowski@dcb.unibe.ch.

Received for review April 8, 2011 and accepted June 2, 2011.

**Published online June 02, 2011**
**10.1021/nn201307g**

4-chloro-phenyl-isocyanide (CPI) monolayers were obtained on Au(111)[22] and Pt (hkl)[23] single crystal facets using gap-mode plasmon excitation in a sandwich structure Me(hkl) | CPI | Au (50 nm) nanoparticles (NPs). This approach was extended toward an electrochemical environment by our group.[24] We demonstrated the tuning of the torsion angle between two aromatic rings in 4,4′-dithiobiphenyl by applying an electrochemical gate field. One step further, Tian *et al.* developed recently an elegant new technique named "shell-isolated nanoparticle enhanced Raman spectroscopy" (SHINERS).[25] The principle of the methods is based on the assembly of a sphere-plane gap-mode system composed of an Au-NPs surrounded by a chemically inert ultrathin and pinhole-free coating of $SiO_2$ in contact with various metal planes or silicon wafers. SHINERS-spectra at an electrified solid | liquid interface were shown for hydrogen adsorbed on Pt-(111) and thiocyanate ions on Au (hkl) from aqueous electrolyte.[25]

In this communication we present an *in situ* SHINERS study for the self-assembly and redox-mediated gating of a viologen-type adlayer on Au(111)-(1×1) single crystal surfaces under electrochemical potential control. Au(60 nm)@$SiO_2$ NPs were employed as "plasmonic antennas". Viologens are obtained by the diquaternizing of 4,4′-bipyridine to *N*,*N*′-dialkyl-4,4′-bipyridinium salts $V^{2+}(X^-)_2$.[26] They received much attention as electron mediators with applications as electron transfer catalysts,[27] electrochromic displays,[28] and solar energy conversion systems in artificial photosynthesis.[29] More recently, viologen derivatives played a key role in the development of molecular-scale devices.[30,31] Examples are rotaxane- or catenane-based electromechanical switches,[32,33] 2D molecular circuits with memory functions,[34] or electrochemical triggered, redox-active single molecular wires.[35−38] The efficiency and uniqueness of viologens in these various settings is related primarily to their facile one-electron reduction of the dication $V^{2+}$ to the radical cation $V^{+\bullet}$, which is unusually stable. The vibrational properties of both and related species on rough metal and thin film electrodes were characterized by *in situ* Raman and infrared spectroscopy at electrified solid | liquid interfaces under a wide range of conditions (*cf.* refs 37,39−46 and references cited therein).

The present paper is the first application of *in situ* SHINERS to an interfacial redox reaction on a well-defined, atomically smooth single crystal electrode under strictly controlled electrochemical conditions. Employing *N*-hexyl-*N*′-(6-mercaptohexyl)-4,4′-bipyridinium bromide (HS-6V6H) on Au(111)-(1×1) as a target system we will show and discuss high quality Raman spectra on surfaces of exactly known and tunable morphology. We will describe adlayer structure−reactivity relations for this redox-switchable system to elucidate the power of SHINERS as a unique *in situ* gap-mode Raman spectroscopy in structure and reactivity studies of a fundamental (electro-) chemical surface science at electrified solid | liquid interfaces down to the nanoscale, and also for a wide range of analytical applications.

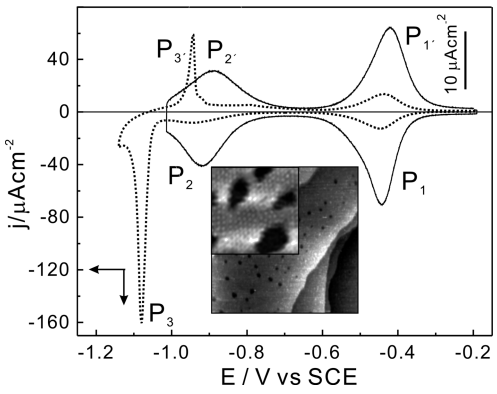


**Figure 1. First scan cyclic voltammograms of Au(111)-(1×1) modified with HS-6V6H electrodes in 0.05 M $KClO_4$, pH adjusted to 10, in −0.200 V > *E* > −1.150 V (start at −0.700 V with a positive scan to −0.200 V, and subsequently scanning toward more negative potentials, dotted line, left current scale) and in −0.200 V (start) > *E* > −1.050 V (solid line, right current scale), sweep rate 50 mV $s^{-1}$. The inset shows an *in situ* STM image of the high coverage HS-6V6H monolayer (100 nm × 100 nm, $E_s$ = −0.200 V, $i_T$ = 50 pA) and a magnification of the locally ordered (√7 × √7) adlayer repeat motif (12 nm × 12 nm, $E_s$ = −0.200 V, $i_T$ = 70 pA).**

## RESULT AND DISCUSSION

Figure 1 shows typical cyclic voltammograms of an ideally smooth, unreconstructed Au(111)-(1×1) electrode modified with a monolayer of HS-6V6H in aqueous 0.05 M $KClO_4$. The pH was ajusted to ∼10 by adding an appropriate amount of KOH. Restricting the potential window to −1.050 V ≤ *E* < −0.200 V (*vs* SCE) results in two pairs of well-resolved current peaks $P_1$ ($E$ = −0.440 V)/$P_1'$($E$ = −0.428 V) and $P_2$ ($E$ = −0.920 V)/$P_2'$($E$ = −0.940 V), which are assigned to the two one-electron redox processes $V^{2+} \leftrightarrow V^{+\bullet}$ and $V^{+\bullet} \leftrightarrow V^0$ of the viologen moiety (Figure 2).[26,37] The coverage is estimated to 3.5 × $10^{-10}$ mol·$cm^{-2}$, which corresponds to an area of 0.47 $nm^2$ per molecule. This value is smaller than the projected area of a planar oriented HS-6V6H molecule (*cf.* crystal structure in ref 47), but larger than the estimated cross section of an all-trans oriented alkanthiol in a densely packed self-assembled monolayer. Extending the potential range to *E* < −1.050 V leads to reductive desorption of the viologen monothiol layer as represented by the cathodic current peak $P_3$. *In-situ* STM showed a high-coverage, poorly ordered adlayer structure of HS-6V6H on Au-(111)-(1×1), even after extended thermal annealing, with characteristic monatomically deep vacancy islands of 2−5 nm. Locally, a (√7 × √7) repeat motif could be identified[37] (*cf.* inset in Figure 1). *In-situ* surface enhanced infrared spectroscopy (SEIRAS) revealed that van-der-Waals interactions between alkyl chains led to

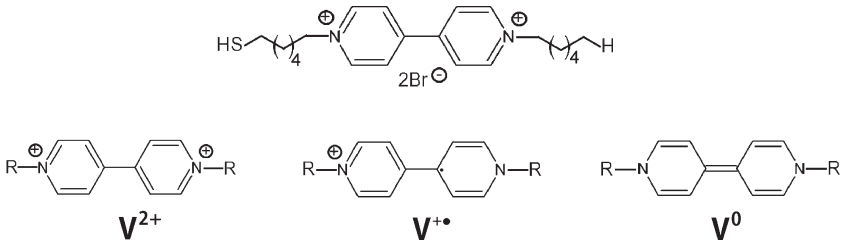


**Figure 2. Molecular structure of *N*-hexyl-*N*′-(6-thiohexyl)-4,4′-bipyridinium bromide (HS-6V6H) and redox states of the viologen core.**

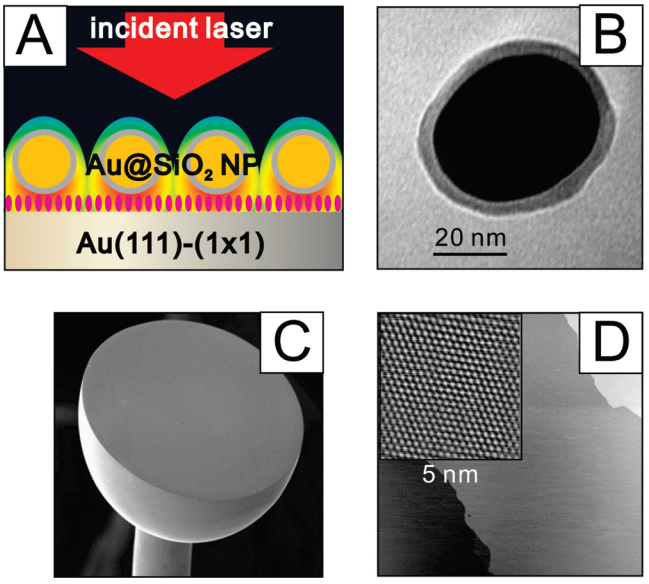


**Figure 3. (A) Schematics of the gap-mode SHINERS configuration. (B) HRTEM image of a typical Au(60 nm)@$SiO_2$ core−shell gold nanoparticle. (C) SEM image of a Clavilier-type Au(111) half-bead crystal employed as working electrode. (D) Large-scale (400 nm × 400 nm) and high-resolution (5 nm × 5 nm) *in situ* STM images of an island-free Au(111)-(1×1) surface ($i_T$ = 0.2 nA respective 0.5 nA, $E_S$ = 0.400 V, in 0.1 M $H_2SO_4$).**

the formation of two hydrophobic layers at the interface with the redox-active $V^{2+}$ moiety enclosed in between.[46] The alkyl chains are aligned in an all-trans conformation with some degree of liquid-like disorder. The long axis of the central $V^{2+}$ unit is tilted with respect to the surface normal. Reduction of $V^{2+} \leftrightarrow V^{+\bullet}$ leads to the radical cation monomer, which might coexist with dimers within the adlayer.[46]

With this background knowledge, the three surface-immobilized HS-6V6H - species $V^{2+}$, $V^{+\bullet}$, and $V^0$ qualify as ideal probes for exploring SHINERS characteristics in redox-active nanojunctions under reaction conditions. The Au(111)-(1×1)|S-6V6H|Au(60 nm)@$SiO_2$ sandwich structure (Figure 3A) was created by assembling first the HS-6V6H molecules on an island-free Au(111)-(1×1) single crystal surface from 1.0 mM ethanolic solution at 60 °C for 12 h in a closed, stainless steel container under argon. Next, $SiO_2$-shelled (~4 nm) Au nanoparticles of ~60 nm diameter were drop-casted onto the Au(111)-S-6V6H surface and dried. The freshly assembled electrode was subsequently transferred into a custom-made spectroelectrochemical cell for *in situ* gap-mode Raman experiments in a back scattering geometry and immediately polarized at $E$ = −0.20 V in 0.05 M $KClO_4$, pH ≈ 10. The electrochemical response of the shelled Au-NPs modified Au(111)-S-6V6H adlayer compares well with the NP-free cyclic voltammogram shown in Figure 1.

Further details on sample preparation and the experimental Raman setup are summarized in the Methods section and the Supporting Information (Figures S1−S3).

Figure 4 displays *in situ* Raman spectra of the redox-active HS-6V6H adlayer on an atomically smooth Au(111)-(1×1) single crystal electrode for selected electrode potentials in the stability range of $V^{2+}$, $V^{+\bullet}$, and $V^0$ in the presence (Figure 4A, SHINERS configuration) as well as in the absence (Figure 4B) of Au(60 nm)@$SiO_2$ NPs. The enhancement of the gap-mode Raman spectra with the shelled NPs is dramatic as compared to the bare viologen monolayer on Au(111)-(1×1). No vibrational signatures could be resolved in the latter case for $V^{2+}$ and $V^0$. $V^0$ appears to decompose rather fast.[41−43] Characteristic bands were only recorded in the stability range of $V^{+\bullet}$ due to

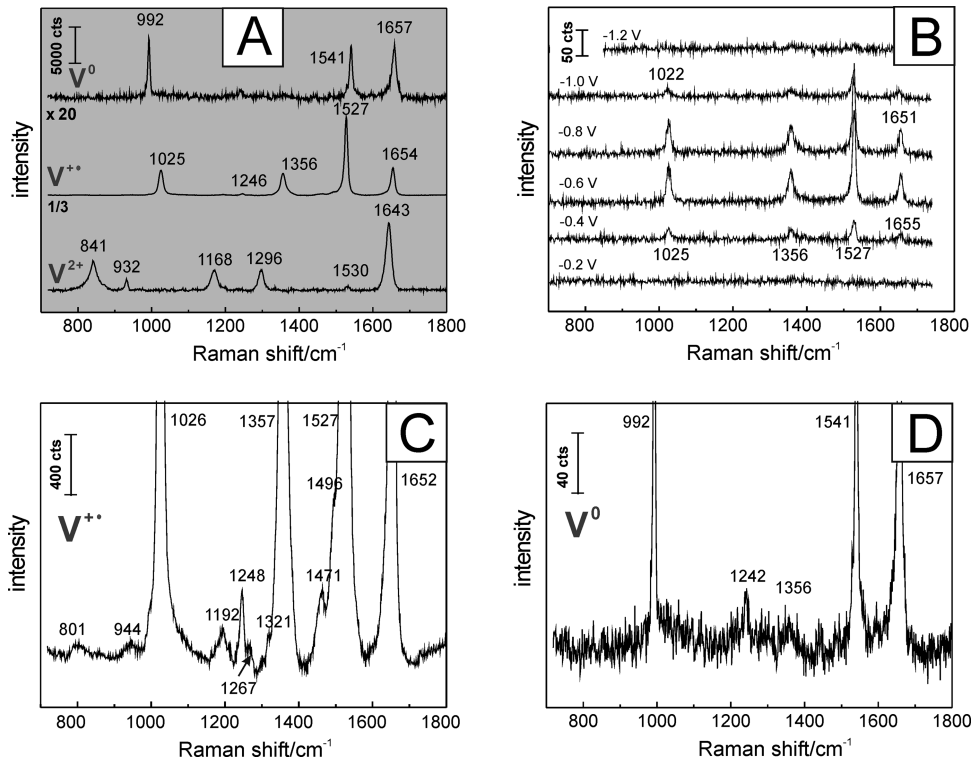


**Figure 4.** *In-situ* **SHINERS (A, C, and D) and resonance Raman spectra (B) of a monolayer of HS-6V6H on an atomically smooth Au(111)-(1×1) electrode in 0.05 M $KClO_4$, pH = 10, for selected electrode potentials in the stability ranges of $V^{2+}$, $V^{+\bullet}$, and $V^0$. The corresponding intensity counts are indicated by the scale bars in all pannels. (A) $V^{2+}$ at $E = -0.100$ V, laser power $P = 1.5$ mW, acquisition time $t_A = 50$ s; $V^{+\bullet}$ at $E = -0.700$ V, $P = 0.15$ mW, $t_A = 5$ s; $V^0$ at $E = -1.05$ V, $P = 0.15$ mW, $t_A = 5$ s. (B) Resonant Raman spectra of the HS-6V6H adlayer on Au(111)-(1×1) in the absence of Au(60 nm)@$SiO_2$ antenna nanoparticles, $P = 0.15$ mW, $t_A = 50$ s. (C and D) Magnification of the SHINERS spectra of $V^{+\bullet}$ and $V^0$ of panel (A) to visualize the nonresonant Raman modes. The laser wavelength was 632.8 nm, and the spot size is estimated as 2 $\mu$m diameter. (For further details see also the Supporting Information.)**

resonance Raman scattering of the radical cation as excited by the 632 nm line of the HeNe laser, which is in resonance with a broad feature in the spectro-electrochemical UV–VIS spectrum (Supporting Information Figure S4 and ref 39,40). The resonance Raman modes are assigned to four totally symmetric fundamental $A_g$-type ring modes assuming a $D_{2h}$ symmetry in the gap (see later and ref 42,43). However, the intensity of these bands is approximately a factor of 3000 smaller (Figure 4B) as compared to the SHINERS spectra. The latter are dominated by a large electromagnetic field enhancement[25] leading to a tremendous increase of the Raman intensity for molecules adsorbed between the Au(60 nm)@$SiO_2$ NPs and the smooth Au(111)-(1×1) surface. Drop-casted and thick core–shell NP films showed similar Raman responses as a "dilute" NP top layer. Furthermore, the four resonant Raman modes in the absence (Figure 4B) as well as in the presence of the SHINERS NPs (Figure 4A) appear at the same positions and show the same potential dependencies. Both observations indicate that the SHINERS NPs act as rather non-invasive probes for the present system under the experimental conditions chosen.

The SHINERS spectra of $V^{2+}$, as recorded at −0.10 V, reveal six well-developed Raman bands in 700 $cm^{-1}$ < $\upsilon$ < 1800 $cm^{-1}$ (Figure 4A). Their assignment is based on a normal coordinate analysis of the vibrational modes of methylviologen and experimental SERS spectra on electrochemically roughened silver electrodes.[42,43] The strong band at 841 $cm^{-1}$ is attributed to a combined C–C and C–N stretching mode of the pyridine ring. The feature at 1168 $cm^{-1}$ is assigned to a N-($CH_2$) stretching vibration with a dominant contribution of the mode between the ring nitrogen and the first methylene group in the alkyl chain.[44] The C–C inter-ring vibration is represented by the band at 1296 $cm^{-1}$. In-plane C–H bending and C–C respective C–N ring modes contribute to the band at 1530 $cm^{-1}$. The strong band at 1643 $cm^{-1}$ reflects C–C inner-ring vibrations. We also observed two rather weak bands at 1062 $cm^{-1}$ and 1242 $cm^{-1}$, which represent a ring breathing stretch and H–C–C angle bending vibrations of the ring (Supporting Information, Figure S5B). All seven bands represent totally symmetric Ag fundamental in-plane vibrations of the $D_{2h}$ point group.[42] Finally, we note that the band at 932 $cm^{-1}$ results from the Cl–O stretching mode of $ClO_4^-$ ions coadsorbed in the $V^{2+}$ adlayer.[46,48]

Potential excursion toward more negative values into the stability range of the radical cation $V^{+\bullet}$ leads

to major changes in the Raman spectrum, which is now characterized by four very strong main bands at 1025, 1356, 1527, and 1654 $cm^{-1}$. The integrated intensities of these Raman bands is typically a factor 200 to 300 larger as compared to the corresponding signals of the viologen dication state $V^{2+}$ (*cf.* Figure 4A and the experimental conditions in the figure captions). Clearly, the enhanced local electromagnetic field in the Au(111)|S-6V6H|Au(60 nm)@$SiO_2$ gap mode configuration couples with the resonance Raman scattering of the radical cation giving rise to a pronounced increase in the detected Raman signals of the redox-active adlayer. The viologen coverage is assumed to be constant, which is supported by previous electrochemical and *in situ* STM data.[37]

The downshift of the ring breathing mode to 1025 $cm^{-1}$ for $V^{+\bullet}$, as compared to $V^{2+}$, indicates that the addition of one electron to the LUMO results in a weakening of the ring C−C bonds as predicted by the extensive nodes, which cross several ring C−C bonds.[41] Considerable electron density is added to the inter-ring C−C vibration upon reduction, which leads to a significant upshift of the frequency to 1356 $cm^{-1}$ at −0.70 V, as compared to 1296 $cm^{-1}$ for $V^{2+}$ at −0.10 V. The strong enhancement of the C−H bending and ring modes at 1527 $cm^{-1}$ reflects the coplanar conformation in $V^{+\bullet}$.[42,49] The Raman bands at 1356 $cm^{-1}$ and 1527 $cm^{-1}$ did not show any time-dependent changes. Only very small satellite peaks could be detected around 1321 $cm^{-1}$ and 1471 $cm^{-1}$ (Figure 4C). Both observations indicate that only a rather small percentage of $(V^{+\bullet})_2$ dimers seems to be favored on rough surfaces as well as upon excitation with a higher energy such as a 514.5 nm argon laser.[39,40] The upshift of the resonance-enhanced mode at 1654 $cm^{-1}$ for $V^{+\bullet}$, as compared to 1643 $cm^{-1}$ for $V^{2+}$, reflects the dominant contributions of the C−C ring vibrations, and rather minor contributions of the inter-ring C−C stretch to this mode.[42] Additional weak bands, which are not in resonance with the HeNe laser excitation (factor 200 to 300 lower in intensity) were detected at 801, 944, 1192, and 1248 $cm^{-1}$ (Figure 4C). The modes at 801 $cm^{-1}$ and 1192 $cm^{-1}$ are dominated by C−N ring-stretch and N-($CH_2$) vibrations. The signature at 944 $cm^{-1}$ represents the coadsorption of $V^{+\bullet}$ with $ClO_4^-$ ions, and the feature at 1248 $cm^{-1}$ is assigned to H−C−C in-plane bending vibrations.[42]

At electrode potentials more negative than $P_2$, for example, $E < -0.900$ V, the viologen adlayer undergoes a second one-electron reduction and the SHINERS spectrum of the fully reduced form $V^0$ is measured. The upper trace in Figure 4A displays data recorded at −1.05 V. We note that the intensities of the SHINERS spectra aquired in the potential region of the neutral viologen form $V^0$ are rather weak. This is not related to the nature of the enhancement mechanism but rather to the decomposition of the molecular adlayer and its superposition with the onset of hydrogen evolution.[37] Nevertheless, the qualitative analysis of the spectra as recorded immediately after changing the electrode potential from −0.700 V to −1.050 V leads to the following observations and conclusions: the spectrum of $V^0$ as plotted in Figure 4A and magnified in panel 4D shows three dominant resonance Raman bands at 992, 1541, and 1657 $cm^{-1}$. The further downshift of the ring breathing mode to 992 $cm^{-1}$ for $V^0$, compared to that of $V^{+\bullet}$ and $V^{2+}$, reflects the weakening of several C−C bonds upon addition of the second electron leading to a quinoid-type structure.[42] The upshift of the band at 1541 $cm^{-1}$ upon reduction to $V^0$ is attributed to the coplanar arrangement of the two rings and to an increase of the force constants of the additionally contributing in-plane C−H bending vibrations.[42] The mode at 1657 $cm^{-1}$ is still dominated by C−C ring vibrations despite a slightly increasing contribution of the inter-ring stretch. Comparison with solution spectra of the three redox forms of methylviologen[50] leads to the conclusion that the formation of $V^0$ is further supported by the absence of a C−N ring stretch around 800 $cm^{-1}$ and the weak inter-ring C−C vibration band around 1356 $cm^{-1}$ (Figure 4D). The weak feature at 1242 $cm^{-1}$ reflects rather unchanged H−C−C in-plane bending mode upon reduction of $V^{+\bullet}$ to $V^0$. The absence of a band in the range between 930 and 940 $cm^{-1}$ demonstrates that perchlorate ions are not coadsorbed with $V^0$ as predicted due to electrostatic reasons.

We also explored the potential-dependent Raman spectra of HS-6V6H adsorbed on an electrochemically roughened gold electrode in a "classical" *in situ* SERS experiment in 0.05 M $KClO_4$, pH ≈ 10, for all three redox forms $V^{2+}$, $V^{+\bullet}$, and $V^0$. The surface-enhanced resonance Raman spectra of the radical cation and of the neutral viologen, as recorded from the adlayer adsorbed on the rough gold surface, are qualitatively identical to the SHINERS spectra obtained from a self-assembled monolayer on the atomically smooth Au(111)-(1×1) electrode. This observation implies that the surface structure has little effect on the resonance Raman signals.

In an attempt to quantify the observed Raman signature and to develop a structure model of the HS-6V6H adlayer on Au(111), we compare in Figure 5 *in situ* SHINERS and SERS spectra of $V^{2+}$ on Au(111) and on a roughened Au(poly) surface, both recorded at −0.10 V, with a crystal powder sample of HS-6V6H. We emphasize that the viologen dication has, under the chosen experimental conditions, no molecular resonance absorption upon excitation with the 632 nm line of the HeNe laser (see also Supporting Information Figure S4). One notices that the intensity of the *in situ* SHINERS and SERS spectra are nearly identical, which demonstrates the pronounced electromagnetic

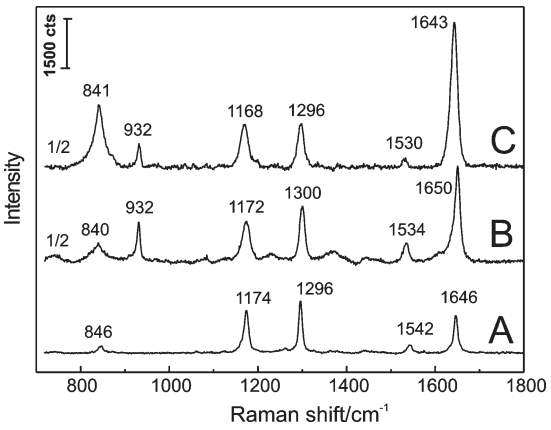


**Figure 5. Raman spectra of the viologen dication $V^{2+}$. (A) Powder spectrum of the bromide salt of HS-6V6H, $P$ = 15 mW, $t_A$ = 1 s. (B) SERS spectrum of a monolayer of HS-6V6H assembled on an electrochemically roughened Au(poly) electrode at $E$ = −0.10 V in 0.05 M $KClO_4$, pH = 10, $P$ = 1.5 mW, $t_A$ = 50 s. (C) SHINERS spectrum of a monolayer of HS-6V6H on Au(111)-(1×1) in 0.05 M $KClO_4$, pH = 10, $P$ = 1.5 mW, $t_A$ = 50 s, $E$ = −0.10 V.**

enhancement of the scattered Raman signal in the structurally well-defined gap-mode configuration Au-(111)-(1×1) | S-6V6H | Au(60 nm)@$SiO_2$ NP. Comparing both spectra with the powder samples enables a rough estimation of the electromagnetic field enhancement factor A as follows:

$$A = \left(\frac{I_{SHINERS}}{N_{SHINERS}}\right) / \left(\frac{I_{bulk}}{N_{bulk}}\right) \quad (1)$$

with $I_i$ being the integrated intensities of the respective Raman signals and $N_i$ being the number of the probed molecules.

The analysis has been carried out for the band around 1168 $cm^{-1}$ assigned to the N-($CH_2$) stretching vibration and the C−C inter-ring vibration around 1296 $cm^{-1}$. Assuming an adlayer coverage of 3.5 × $10^{-10}$ mol $cm^{-2}$, 60 $\mu$m penetration depth of the laser signal into the crystal powder, 2 $\mu$m of the focused beam and a density of the bulk sample amounting to 1.2 to 1.4 g $cm^{-3}$,[47,51] we estimate for both the SHINERS and the SERS spectra of $V^{2+}$ as shown in Figure 5 an enhancement factor $A$ of the order of 3 × $10^5$ (see Supporting Information for details). Under resonance conditions, as in the case of $V^{+\bullet}$ and $V^0$, this value increases by more than 2 orders of magnitude.

The observation of strong Raman bands in the SHINERS and SERS spectra and the bulk crystal spectrum of $V^{2+}$, which have polarizability changes perpendicular to each other (Figures 4 and 5, and ref 42) allow the use of the surface selection rule[6] to estimate the orientation of the viologen ring relative to the surface normal. Because of the relative (electromagnetic) enhancement of the components of the optical field, which is perpendicular to the surface, over that which is parallel to the surface, those modes generating polarizability changes perpendicular to the surface are enhanced relative to those which produce polarizability changes parallel to the surface. The following analysis will be rather qualitative because more than one mode contributes to the observed bands, which precludes a quantitative treatment.

For the purpose of discussion, we introduce a Cartesian coordinate system (Figure 6A). The long axis of the viologen moiety is aligned with the z-direction. The band at 1168 $cm^{-1}$, which is mainly derived from the N-($CH_2$) stretch between the ring nitrogen and the first methylen group in the chain[42,44] is taken as internal reference. The predominant component of the polarizability change of this mode is along the $z$-axis of the chosen coordinate system. The intensity ratios of the main bands around 841 $cm^{-1}$ ($A_{g1}$), 1296 $cm^{-1}$ ($A_{g2}$), and 1643 $cm^{-1}$ ($A_{g3}$) with respect to the N-($CH_2$) stretch $A_{g,ref}$ of each spectrum shown in Figure 5 are summarized in Table 1.

The ratios $I_{Ag2}/I_{Ag,ref}$ of the powder and of the two surface spectra shown in Figure 5 are identical and amount approximately to 1. This result is expected because the band around 1296 $cm^{-1}$ ($A_{g2}$) is dominated by the C−C inter-ring stretch, which has a polarizability change directly along the $z$-axis. The ratios $I_{Ag1}/I_{Ag,ref}$ and $I_{Ag3}/I_{Ag,ref}$ increase significantly from the bulk sample to spectra recorded in the SHINERS configuration and approach a value of up to 2.5 for the latter case, which is more than twice the ratio $I_{Ag2}/I_{Ag,ref}$. The bands around 841 $cm^{-1}$ ($A_{g1}$) and 1643 $cm^{-1}$ ($A_{g3}$) are mainly derived from in-plane C−C and C−N stretches of the atoms within the ring system, which leads to polarizability changes with non-negligible components also perpendicular to the main molecular $z$-axis. The ratios of the integrated intensities $I_{Ag1}/I_{Ag,ref}$ and $I_{Ag3}/I_{Ag,ref}$ of the monolayer samples acquired in the SHINERS and SERS experiments are higher as compared to those for the isotropic (*i.e.*, unoriented) bulk sample. This trend indicates clearly a higher degree of orientational order in the monolayer samples, with a particularly higher order in the SHINERS configuration Au(111) | S-6V6H | Au(60 nm)@$SiO_2$. This result reflects also the atomically smooth single crystal surface in the latter experiment.

Considering the surface selection rule[6] and the predominant alignment of the polarizability changes of $A_{g,ref}$ and $A_{g2}$ with the long molecular axis, this trend clearly indicates that the viologen moiety is not upright oriented with respect to the substrate surface but assumes an edge-on tilted orientation in the self-assembled monolayer on Au(111)-(1×1). In other words, the molecular $z$-axis is inclined with respect to the surface normal and the main components of the polarizability changes of the C−C and C−N ring modes are not aligned parallel to the surface. This conclusion is in agreement with *in situ* electroreflectance and infrared studies.[46,52] Sagara *et al.*[52] estimated for HS-4 V4H on Au(poly) 65° as a tilt angle of the viologen

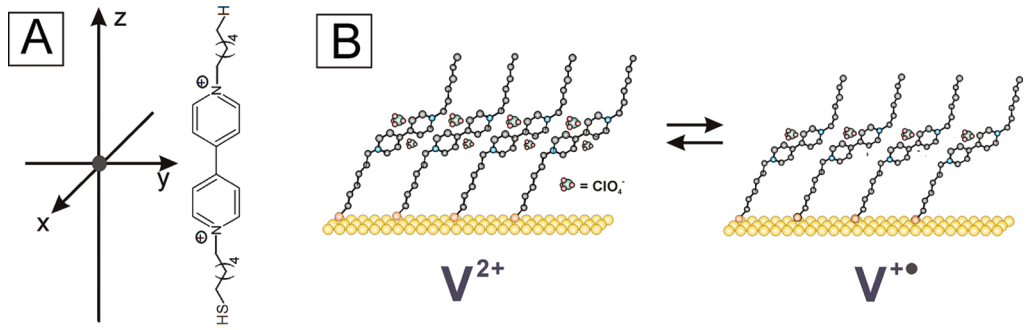


**Figure 6. (A) Cartesian coordinate system and alignment of molecular axes in HS-6V6H. (B and C) Structure models of the $V^{2+}$ and $V^{+\bullet}$ adlayers of of HS-6V6H on Au(111)-(1×1) in 0.05 M $KClO_4$.**

**TABLE 1. Estimated Ratios of the Integrated Intensities $I_i$ of the Bands $A_{g1}$ (C−C and C−N Stretch ~841 $cm^{-1}$), $A_{g2}$ (C−C Inter-ring Stretch around 1296 $cm^{-1}$), and $A_{g3}$ (C−C Ring Stretch around 1643 $cm^{-1}$)[42] with Respect to the Internal Reference Band $A_{g,ref}$ around 1168 $cm^{-1}$**

| method | $A_{g,ref}$ ($cm^{-1}$) | $I_{Ag1}/I_{Ag,ref}$ | $I_{Ag2}/I_{Ag,ref}$ | $I_{Ag3}/I_{Ag,ref}$ |
|---|---|---|---|---|
| SHINERS | 1168 | ~2 | ~1 | 2.5 |
| SERS | 1172 | ~0.7 | ~1 | 2 |
| bulk crystal | 1174 | ~0.25 | ~1 | 1 |

moiety as well as a tilt angle of 30° of the all-trans alkyl chain attached to the gold electrode *via* the thiol linker. Our previous infrared study revealed that the methylene chain environment of the high coverage HS-6V6H adlayer on Au(111−25 nm) film electrodes is liquidlike, that is, there exists a certain degree of conformational disorder in the 2D assembly.[46] On the other hand, Tang *et al.*[44] suggested from infrared and SERS experiments a perpendicular orientation of the ring system in HS-10 V10H on a roughened gold electrode.

Based on the SHINERS data described above (Figure 4 and Figure 5), in combination with the electrochemical *in situ* STM (Figure 1) and infrared experiments,[46] we propose the following sandwich model of the HS-6V6H adlayer on Au(111) (Figure 6B): The alkyl chains attached to the gold surface *via* the thiol anchor are aligned in an all-trans conformation assuming a tilt angle of 20 to 30° with respect to the surface normal. The long axis of the edge-on oriented viologen moiety is tilted even further. Packing considerations, based on the locally resolved ($\sqrt{7} \times \sqrt{7}$) repeat pattern in the *in situ* STM experiments (Figure 1), suggest values ranging between 40° and 70°. van der Waals interactions between the alkyl chains lead to two hydrophobic layers with the redox-active bipyridinium moiety $V^{2+}$ aligned in between. The alkyl chains facing the electrolyte appear to be more disordered ("liquidlike") due to packing constraints. The positive charges of the $V^{2+}$ cation are balanced by coadsorbed $ClO_4^-$ anions, most probably located close to the ring nitrogen atoms. The spatial arrangement of the $V^{2+}$ cation in edge-on orientation is stabilized by interplanar $\pi-\pi$ stacking. Dominant $\pi-\pi$ stacking between the pyridyl rings reduces the force constants in the C−C ring stretch modes. Indeed, the stacking "marker" band $A_{g3}$[42,53] shows a significant red shift from 1650 $cm^{-1}$ for the adlayer on the roughened gold surface to 1643 $cm^{-1}$ for the self-assembled monolayer on the single crystal Au(111) electrode (Figure 5).

The above model is consistent with all experimental observations and provides sufficient evidence for abandoning the earlier proposal of Tang *et al.*[44] The open structure as suggested in our present study is enforced by the bulky size of the tilted viologen moiety, which prevents a more compact alignment of the alkyl chains, such as a ($\sqrt{3} \times \sqrt{3}$)R30 for a well-ordered alkyl monolayer on Au(111).[54]

Superposition of the electromagnetic field enhancement with a resonance Raman effect, which is difficult to deconvolute and to quantify, prevents a similar detailed analysis for the radical cation $V^{+\bullet}$. However, the high reversibility of the voltammetric and spectroscopic responses in combination with the unchanged local ($\sqrt{7} \times \sqrt{7}$) *in situ* STM contrast pattern upon the potential-induced transition $V^{2+} \leftrightarrow V^{+\bullet}$ suggests that the overall alignment of alkyl chains and viologen moiety in the interfacial adlayers of the two redox states is rather similar. We just notice a decrease in the amount of coadsorbed $ClO_4^-$ (Figure 4C) and the coexistence of a (small) amount of $(V^{+\bullet})_2$ dimers in the $V^{+\bullet}$ adlayer (Figure 4C, Figure 6).

We refrain from proposing a structure model for $V^0$ on Au (111). The adlayer is not in a steady state in the entire accessible potential window due to decomposition[41] and onset of desorption.[37]

Finally, we illustrate the robustness of the viologen-based redox switching reaction $V^{2+} \leftrightarrow V^{+\bullet}$. We cycled the electrode potential more than 500 times between −0.200 V and −0.700 V, and recorded simultaneously the voltammetric and Raman responses. Figure 7 illustrates, as an example, six potential cycles of this sequence (see also Figure S7 in SI). The Raman

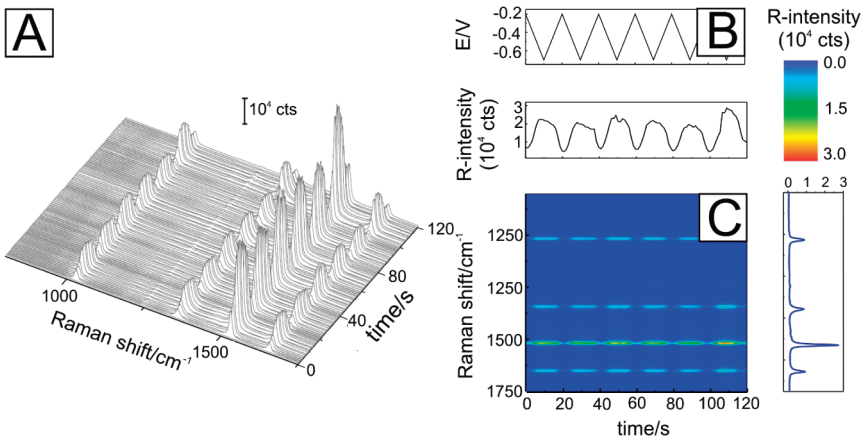


**Figure 7. Example of SHINERS spectra of six potentio-dynamic cycles between −0.200 and −0.700 V, 50 mV $s^{-1}$, for the reversible transition between $V^{2+}$ and $V^{+\bullet}$, $P = 0.3$ mW, $t_A = 1$ s. (A) 3D Raman spectrum during potential cycling; (B) potential cycling sequence and corresponding evolution of the intensity profile of the $A_g$ mode ≈ 1527 $cm^{-1}$; (C) Raman intensity contour plot as constructed from data shown in panel A. The four Raman bands resolved in panels A and C represent the characteristic $A_g$ resonance Raman modes of $V^{+\bullet}$ (*cf.* Figure 4).**

intensities of the four $A_g$-type resonance Raman bands of $V^{+\bullet}$ appear and increase during the negative-going half cycle −0.20 → −0.700 V. The reformation of the dication $V^{2+}$ during the following return half-cycle to −0.200 V leads to the quenching of the $V^{+\bullet}$ response. The 3D representation as well as the intensity contour map, plotted in Figure 7A,C, illustrates the potential-dependent modulation of the $V^{+\bullet}$-related Raman signals. Both graphs demonstrate the potential-driven evolution of the $V^{2+}$ ↔ $V^{+\bullet}$ equilibrium or, in other words, the potential-dependent composition of the redox-active molecular adlayer. The time- and potential-dependent evolution of the spectroscopic response also demonstrates that the entire electrochemical reaction involved is completely reversible. Finally we note that the nonresonant signals related to $V^{2+}$ and $V^{+\bullet}$ (*cf.* Figure 4 and Supporting Information, Figure S5) are not "visible" in Figure 7 due to their low intensity (a factor of 200−300 smaller as compared to the resonance Raman enhanced modes).

Our data illustrate nicely the uniqueness and stability of the redox-active adlayer and the potential of the fundamental $V^{2+}$ ↔ $V^{+\bullet}$ unit for applications as bistable electrical/electrochemical or electro-optical switching respective recognition element.

## CONCLUSIONS

We reported in this paper the first application of *in situ* SHINERS to an interfacial redox reaction under strictly controlled electrochemical conditions. We constructed a gap-mode sandwich structure composed of the thiol-terminated HS-6V6H viologen derivative immobilized on a single crystal Au(111)-(1×1) electrode and covered by Au(60 nm)@$SiO_2$ core−shell nanoparticles as plasmonic antennas. We observed high-quality, potential-dependent Raman signals of the three viologen species $V^{2+}$, $V^{+\bullet}$, and $V^0$ on a well-defined smooth Au(111) substrate surface, and could map their potential-dependent evolution. Comparison with experiments on powder samples revealed an enhancement factor of the nonresonant Raman modes of ~$3 \times 10^5$, and up to $9 \times 10^7$ for the resonance modes. These intensities appear to be comparable with data obtained under "classical" SERS conditions.

As an example, we investigated details of the adlayer structure and spectra evolution of the potential-induced reversible switching between the viologen dication $V^{2+}$ and the radical cation $V^{+\bullet}$ generated upon uptake of an electron. The latter shows resonance and nonresonance Raman bands of unprecedented intensities. The resonance Raman modes were chosen as marker bands to demonstrate the remarkable stability of the viologen-based redox switch.

This study illustrates the unique potential of SHINERS in the entire field of electrochemical surface science to explore structures and reaction pathways on well-defined substrate surfaces, such as single crystals, for molecular, (electro-)catalytic, bioelectrochemical systems up to fundamental double layer studies at electrified solid | liquid interfaces.

## METHODS

**Materials.** The electrolyte solutions were prepared with Milli-Q water (18 MΩ·cm, 2 ppb TOC), $KClO_4$ (Fluka puriss p.a., twice recrystallized from water), KCl (Merck, p.a.), HCl (suprapure Merck), KOH (suprapure Merck), and ethanol (p.a., KMF). All electrolytes were deaerated with 5 N argon (Carbagas) before and during the experiments. The measurements were carried out at 20 ± 0.5 °C. Glassware and Kel-F cells were cleaned either in caroic acid or in a 1:1 mixture of hot $H_2SO_4$ (95−97%,

pro-analysis, Merck) and $HNO_3$ (65% purissimum, Riedel-de-Haen), followed by extended rinsing with Milli-Q water.

The synthesis of 6-hexyl-6′-(*n*-thiohexyl)-4,4′-bipyridinium bromide (HS-6V6H) and purification protocols are described in ref 37.

**Preparation of the Gold Working Electrodes.** The electrodes used were Clavilier-type hemispherical single crystalline Au(111) bead electrodes (typically 2 to 3 mm diameter) with a gold wire attached to the rear for mounting (Figure 3C), or polycrystalline Au(poly) disk electrodes, 2 mm diameter embedded into a 6 mm Teflon cover (BAS).

The preparation of island-free, unreconstructed Au (111)-(1×1) electrodes (Figure 3D) followed a procedure previously described in ref 55. In short: The electrode was annealed in a butane flame at bright red heat for ~5 min and then cooled in an argon atmosphere down to room temperature. Then the flame-annealed Au(111)-($p\times\sqrt{3}$) electrode was immersed into 25 mM HCl for 10 min in order to lift the reconstruction and to create island-free Au (100)-(1×1) surfaces with rather large (1×1) terraces for subsequent surface modification. Chloride ions were removed by rinsing the electrode with copious amounts of Milli-Q water and drying in a stream of argon in a protecting tube.

The preparation of Raman-active rough surfaces of the Au(poly) disk electrodes followed a procedure introduced by Weaver *et al.*[56] In short, the Au(poly) electrode was first mechanically polished with 1 $\mu$m and subsequently 0.05 $\mu$m aluminum powder down to a mirror finish followed by careful rinsing and ultrasonic cleaning with Milli-Q water. Next, the electrode was transferred into an electrochemical cell filled with 0.1 aqueous M KCl. The electrode was first polarized at −0.3 V *versus* SCE and then its potential was scanned with 1 V $s^{-1}$ to +1.25 V *versus* SCE, where the potential was held for 1.5 s. The cycle was completed by scanning the potential back to −0.30 V with 0.5 V $s^{-1}$. After 30 s reduction time at this potential, the roughened electrode was removed from the electrolyte, carefully rinsed with Milli-Q water, dried, and subsequently employed for surface modification with HS-6V6H.

**Core−Shell Au Nanoparticles.** Au nanoparticles with a diameter of ~55 nm were synthesized by reducing 200 mL of a boiling (under reflux) 0.01 wt % $HAuCl_4$ (Sigma, 99.99%) solution with 1.5 mL of 1 wt % sodium citrate (Alfa Aesar, 99.9%) following Frens procedure.[57] Upon cooling, the Au sol was concentrated *via* centrifugation (20%). Next, 0.4 mL of a freshly prepared 1.0 mM aqueous solution of (3-aminopropyl) trimethoxysilane (Alfa Aesar, 97%) were added to 30 mL of the gold sol under vigorous stirring during 15 min ensuring the complete complexation of the amine groups with the gold surface. Then 3.2 mL of 0.54 wt % sodium silicate solution (Sigma-Aldrich, reagent grade, pH ≈ 10.28) were added to the sol under vigorous stirring during 3 min. Subsequently, the reaction mixture was kept at 90 °C for 60 min to form high-quality Au(60 nm)@$SiO_2$ core−shell nanoparticles with an ultrathin and pinhole free silicon shell (for characterization details see Supporting Information Figures S1−S3).[25,58,59]

**Self-assembled HS-6V6H monolayers on gold electrodes.** The viologen (HS-6V6H) monolayers were prepared by immersing the Au(111)-(1×1) single crystal electrodes or the roughened Au-(poly) disk electrodes in 1.0 mM ethanolic solution of HS-6V6H, followed by thermal annealing at 60 °C for 6 h to create ordered high-coverage adlayers. The thermal treatment was performed in the absence of oxygen in a stainless steel autoclave to prevent the evaporation of ethanol.[37] After self-assembly, the modified Au-electrodes were rinsed with warm ethanol to remove physisorbed viologen species and dried in a stream of argon. For the preparation of the Au(111)-(1×1) | S-6V6H | Au-(60 nm)@ $SiO_2$ NP sandwich assembly 2 $\mu$L of the core−shell NP in water were drop-casted onto the modified gold electrode and dried. A rather "dilute" NP top layer was obtained by gentle rinsing with water.

**Electrochemistry.** The electrochemical characterization of the bare and adsorbate-modified gold electrodes was performed in a three-compartment glass cell with an Autolab PG30 Workstation (Metrohm). A saturated calomel electrode (SCE) and a platinum coil served as reference and counter electrodes, respectively. All potentials given in this paper refer to the SCE potential scale (if not stated explicitely otherwise). Electrochemical STM measurements were carried out with a Molecular Imaging PicoSPM. Further details are given in ref 37.

**Raman Measurements.** *In situ* SERS measurements were carried out on a LabRAM HR800 confocal microscope Raman system (Horiba Jobin Yvon). The excitation wavelength is 632.8 nm from a He−Ne laser. The microscope objective for laser illumination and signal collection was of long working distance (8 mm) with 50× magnification and a numerical aperture of 0.5. The custom-made spectroelectrochemical flow-cell was equipped with a Pt counter electrode and Ag/AgCl double junction reference electrode, and several ports for solution exchange and deareation. The electrolyte solutions were deaerated by argon gas before injected to the spectroelectrochemical cell through Teflon tubes. All experiments were performed at room temperature.

*Acknowledgment.* The authors acknowledge the advice of Dr. J. F. Li, and the expert help of U. Linke, Research Center Jülich, for preparing the single crystal gold electrodes used in this study. The authors are also grateful to the Swiss National Science Foundation (200021_124643; 200020_122069, Sinergia CRSII2_126969; NFP 62 406240_126 108) and the ITN FP7 Network FUNMOLS for financial support.

*Supporting Information Available:* Au and Au@$SiO_2$ nanoparticle characterization, UV−vis spectroelectrochemical data of HS-6V6H on gold electrodes, enlarged Raman spectra, and estimation of the enhancement factor. This material is available free of charge *via* the Internet at http://pubs.acs.org.

## REFERENCES AND NOTES

1. Fleischmann, M; Hendra, P. J.; McQuillan, A. J. Raman-Spectra of Pyridine Adsorbed at a Silver Electrode. *Chem. Phys. Lett.* **1974**, *26*, 163–166.
2. Jeanmaire, D. L.; Van Duyne, R. P. Surface Raman Spectroelectrochemistry: Part I. Heterocyclic, Aromatic, and Aliphatic Amines Adsorbed on Anodized Silver Electrode. *J. Electroanal. Chem.* **1977**, *84*, 1–20.
3. Albrecht, M. G.; Creighton, J. A. Anomalously Intense Raman Spectra of Pyridine at a Silver Electrode. *J. Am. Chem. Soc.* **1977**, *99*, 5215–5217.
4. Tian, Z. Q.; Ren, B.; Li, J. F.; Yang, Z. L. Expanding Generality of Surface-Enhanced Raman Spectroscopy with Borrowing SERS Activity Strategy. *Chem. Commun.* **2007**, *34*, 3514–3534.
5. Wu, D. Y.; Li, J. F.; Ren, B.; Tian, Z. Q. Electrochemical Surface-Enhanced Raman Spectroscopy of Nanostructures. *Chem. Soc. Rev.* **2008**, *37*, 1025–1041.
6. Moskovits, M. Surface-Enhanced Spectroscopy. *Rev. Mod. Phys.* **1985**, *57*, 783–826.
7. Schatz, G. C.; Young, M. A.; Van Duyne, R. P. Electromagnetic Mechanism of SERS. *Top. Appl. Phys.* **2006**, *103*, 19–46.
8. Moskovits, M. Surface-Enhanced Raman Spectroscopy: A Brief Perspective. *Top. Appl. Phys.* **2006**, *103*, 1–18.
9. Creighton, J. A.; Blatchford, C .G.; Albrecht, M. G. Plasma Resonance Enhancement of Raman Scattering by Pyridine Adsorbed on Silver or Gold Sol Particles of Size Comparable to the Excitation Wavelength. *J. Chem. Soc., Faraday Trans. 2* **1979**, *75*, 790–798.
10. Wetzel, H.; Gerischer, H.; Pettinger, B. Comparison of Potential Dependence of the Surface-Enhanced Raman Effect at Colloid Silver Particles and Bulk Silver Electrode. *Chem. Phys. Lett.* **1982**, *85*, 187–189.
11. Nikobakht, B.; Wang, J.; El-Sayed, M. A. Surface-Enhanced Raman Scattering of Molecules Adsorbed on Gold Nanorods: Off-Surface Plasmon Resonance Condition. *Chem. Phys. Lett.* **2002**, *366*, 17–23.
12. Park, S.; Yang, P. X.; Corredor, P.; Weaver, M. J. Transition Metal-Coated Nanoparticle Films: Vibrational Characterization with Surface-Enhanced Raman Scattering. *J. Am. Chem. Soc.* **2002**, *124*, 2428–2429.

13. Tian, Z. Q.; Ren, B.; Wu, D. Y. Surfaced-Enhanced Raman Scattering: From Noble to Transition Metals and from Rough Surfaces to Ordered Nanostructures. *J. Phys. Chem. B* **2002**, *106*, 9463–9483.
14. Willets, K. A.; Van Duyne, R. P. Localized Surface Plasmon Spectroscopy and Sensing. *Annu. Rev. Phys. Chem.* **2007**, *58*, 267–297.
15. Mahajan, S.; Abdelsalam, M.; Suguwara, Y.; Cintra, S.; Russell, A.; Baumberg, J.; Bartlett, P. Tuning Plasmons on Nanostructured Substrates for NIR-SERS. *Phys. Chem. Chem. Phys.* **2007**, *9*, 104–109.
16. Baumberg, J. J.; Kelf, T. A.; Sugawara, Y.; Cintra, S.; Abdelsalam, M. E.; Bartlett, P. N.; Russell, A. E. Angle-Resolved Surface-Enhanced Raman Scattering on Metallic Nanostructured Plasmonic Crystals. *Nano Lett.* **2005**, *5*, 2262–2267.
17. Bruckbauer, A.; Otto, A. Raman Spectroscopy of Pyridine Adsorbed on Single Crystal Copper Electrodes. *J. Raman Spectrosc.* **1998**, *29*, 665–672.
18. Pettinger, B.; Ren, B.; Picardi, G.; Schuster, R.; Ertl, G. Nanoscale Probing of Adsorbed Species by Tip-Enhanced Raman Spectroscopy. *Phys. Rev. Lett.* **2004**, *92*, 096101.
19. Ren, B.; Piccardi, G.; Pettinger, B.; Schuster, R.; Ertl, G. Tip-Enhanced Raman Spectroscopy of Benzenethiol Adsorbed on Au and Pt Single Crystal Surfaces. *Angew. Chem., Int. Ed.* **2005**, *44*, 139–142.
20. Liu, Z.; Wang, X.; Dai, K.; Jin, S.; Zeng, Z. C.; Zhuang, M. D.; Yang, Z. L.; Wu, D. Y.; Ren, B.; Tian, Z. Q. Tip-Enhanced Raman Spectroscopy for Investigating Adsorbed Nonresonant Molecules on Single-Crystal Surfaces: Tip Regeneration, Probe Molecule, and Enhancement Effect. *J. Raman Spectrosc.* **2009**, *40*, 1400–1406.
21. Pettinger, B., *personal communication,* 2010.
22. Ikeda, K.; Fujimoto, N.; Uehara, H.; Uosaki, K. Raman Scattering of Aryl Isocyanide Monolayers on Atomically Flat Au(111) Single Crystal Surfaces Enhanced by Gap-Mode Plasmon Excitation. *Chem. Phys. Lett.* **2008**, *460*, 205–208.
23. Ikeda, K.; Sato, J.; Fujimoto, N.; Hayazawa, N.; Kawata, S.; Uosaki, K. Plasmonic Enhancement of Raman Scattering on Non-SERS-Active Platinum Substrates. *J. Phys. Chem. C* **2009**, *113*, 11816–11821.
24. Cui, L.; Liu, B.; Vonlanthen, D.; Mayor, M.; Fu, Y. C.; Li., J. F.; Wandlowski, Th. *In-Situ* Gap-Mode Raman Spectroscopy on Single Crystal Au(100) Electrodes: Tuning the Torsion Angle of 4,4′-Biphenyldithiols by an Electrochemical Gate Field. *J. Am. Chem. Soc.* **2011**, *133*, 7332–7335.
25. Li, J. F.; Huang, Y. F.; Ding, Y.; Yang, Z. L.; Li, S. B.; Zhou, X. S.; Fan, F. R.; Zhang, W.; Zhou, Z. Y.; Wu, D. Y.; ; *et al.* Shell-Isolated Nanoparticle-Enhanced Raman Spectroscopy. *Nature* **2010**, *464*, 392–395.
26. Monk, P. M. S. The Viologens: Physicochemical Properties, Synthesis and Applications of the Salts of 4,4′-Bipyridine. John Wiley & Sons: Chichester, U.K., 1998.
27. Goren, Z.; Willmer, I. Photochemical and Chemical Reduction of Vicinal Dibromides *via* Phase Transfer of 4,4′-Bipyridinium Radical: The Role of Radical Disproportionation. *J. Am. Chem. Soc.* **1983**, *105*, 7764–7765.
28. Vergaz, R.; Barrios, D.; Sanchez-Pena, J. M.; Pozo-Gonzalo, C.; Salsamendi, M. Relating Cyclic Voltammetry and Impedance Analysis in a Viologen Electrochromic Device. *Sol. Energy Mater. Sol. Cells* **2009**, *93*, 2125–2132.
29. Hu, Y. Z.; Tsukiji, S.; Shinkai, S.; Oishi, S.; Hamachi, I. Construction of Artificial Photosynthetic Reaction Centers on a Protein Surface: Vectorial, Multistep, and Proton-Coupled Electron Transfer for Long-Lived Charge Separation. *J. Am. Chem. Soc.* **2000**, *122*, 241–253.
30. Saha, S.; Stoddart, J. F. Photo-Driven Molecular Devices. *Chem. Soc. Rev.* **2007**, *36*, 77–92.
31. Raymo, F. M.; Alvarado., R. J.; Pacsial, E. J. Electroactive Films Incorporating 4,4-Bipyridinium Building Blocks. *J. Supramol. Chem.* **2002**, *2*, 63–67.
32. Collier, C. P.; Mattersteig, G.; Wang, E. W.; Luo, Y.; Beverley, K.; Sampaio, J.; Raymo, F. M.; Stoddart, J. F.; Heath, J. R. A [2]Catenane-Based Solid State Electronically Reconfigurable Switch. *Science* **2000**, *289*, 1172–1175.
33. Trabolsi, A.; Khashab, N.; Fahrenbach, A. C.; Friedman, D. C.; Colvin, M. T.; Coti, K. K.; Benitez, D.; Tkatchouk, E.; Olsen, J. C.; Belowich, M. E.; ; *et al.* Radically Enhanced Molecular Recognition. *Nat. Chem.* **2010**, *2*, 42–49.
34. Luo, Y.; Collier, C. P.; Jeppeson, J. O.; Nielsen, K. A.; Delonno, E.; Ho, G.; Perkins, J.; Tseng, H. R.; Yamamoto, T.; Stoddard, J. F.; ; *et al.* Two-Dimensional Molecular Electronics Circuits. *Chem. Phys. Chem.* **2002**, *3*, 519–525.
35. Gittins, D. I.; Bethell, D.; Schiffrin, D. J.; Nichols, R. J. A Nanometre-Scale Electronic Switch Consisting of a Metal Cluster and Redox-Addressable Groups. *Nature* **2000**, *408*, 67–69.
36. Haiss, W.; van Zalinge, H.; Higgins, S. J.; Bethell, D.; Hobenreich, H.; Schiffrin, D. J.; Nichols, R. J. Redox State Dependence of Single Molecule Conductivity. *J. Am. Chem. Soc.* **2003**, *125*, 15294–15295.
37. Li, Z.; Han, B.; Meszaros, G.; Pobelov, I.; Wandlowski, Th.; Blaszczyk, A.; Mayor, M. Two-Dimensional Assembly and Local Redox-Activity of Molecular Hybrid Structures in An Electrochemical Environment. *Faraday Discuss.* **2006**, *131*, 121–143.
38. Pobelov, I.; Li, Z.; Wandlowski, Th. Electrolyte Gating in Redox-Active Tunneling Junctions—An Electrochemical STM Approach. *J. Am. Chem. Soc.* **2008**, *130*, 16045–16054.
39. Osawa, M.; Nishijima, K.; Suetaka, W. Potential Modulation Raman-Spectroscopy for *in-situ* Observation of the Electrode−Electrolyte Interface. *Surf. Sci.* **1981**, *104*, 270–281.
40. Osawa, M.; Suetaka, W. Electrochemical Reduction of Heptyl Viologen at Platinum Studied by Time-Resolved Resonance Raman Spectroscopy. *J. Electroanal. Chem.* **1989**, *270*, 261–272.
41. Lu, T. H.; Cotton, T. M. *In Situ* Raman-Spectra of the Three Redox Forms of Heptylviologen at Platinum and Silver Electrodes—Counter Ion Effects. *J. Phys. Chem.* **1987**, *91*, 5978–5985.
42. Ghoshal, S.; Lu, T. H.; Feng, Q.; Cotton, T. M. A Normal Coordinate Analysis of the Vibrational Modes of the 3 Redox Forms of Methylviologen—Comparison with Experimental Results. *Spectrochim. Acta, Part A* **1988**, *44*, 651–660.
43. Lu, T. H.; Cotton, T. M.; Hurst, J. K.; Thompson, D. H. P. A Raman and Surface-Enhanced Raman-Study of Asymmetrically Substituted Viologens. *J. Phys. Chem.* **1988**, *92*, 6978–6985.
44. Tang, X. Y.; Schneider, T.; Buttry, D. A. A Vibrational Spectroscopic Study of the Structure of Electroactive Self-Assembled Monolayers of Viologen Derivatives. *Langmuir* **1994**, *10*, 2235–2240.
45. Tang, X. Y.; Schneider, T. W.; Walker, J. W.; Buttry, D. A. Dimerized $\pi$-Complexes in Self-Assembled Monolayers Containing Viologens: An Origin of Unusual Wave Shapes in the Voltammetry of Monolayers. *Langmuir* **1996**, *12*, 5921–5933.
46. Han, B.; Li, Z.; Wandlowski, Th.; Blaszczyk, A.; Mayor, M. Potential-Induced Redox Switching in Viologen Self-Assembled Monolayers: An ATR-SEIRAS Approach. *J. Phys. Chem. C* **2007**, *111*, 13855–13863.
47. Polishchuk, I. Y.; Grineva, L. G.; Polishchuk, A. P.; Chernega, A. N. Ionic Donor−Acceptor Complexes. Effect of Electron-Donor Anion Properties on the Structure of 4,4′-Dipyridinium Dications. *Zh. Obshch. Khim.* **1996**, *66*, 1530–1536.
48. Tian, Z. Q.; Mao, B. W.; Gao, J. S. Surface-Enhanced Raman-Spectroscopic Studies on Structural Dynamics of Coadsorption of Thiourea and $ClO_4^-$ at Silver Electrodes. *J. Electroanal. Chem.* **1994**, *379*, 271–279.
49. Hester, R. E.; Suzuki, S. Vibrational Analysis of Methylviologen. *J. Phys. Chem.* **1982**, *86*, 4626–4630.
50. Feng, Q.; Cotton, T. M. A Surface-Enhanced Resonance Raman Study of the Photoreduction of Methylviologen on a p-Indium Phosphide Semiconductor Electrode. *J. Phys. Chem.* **1986**, *90*, 983–987.
51. Grineva., I.; Krainov, I.; Polishchuk, A.; Tomachev, M. Effect of the Solid Phase Structure Upon Photochromic Properties of 4,4′-Bipyridine Derivatives. *Mol. Cryst. Liq. Cryst.* **1992**, *211*, 397–402.

52. Sagara, T.; Maeda, H.; Yuan, Y.; Nakashima, N. Voltammetric and Electroreflectance Study of Thiol-Functionalized Viologen Monolayers on Polycrystalline Gold: Effect of Anion Binding to a Viologen Moiety. *Langmuir* **1999**, *15*, 3823–3830.
53. Osawa, M; Yoshi, K. *In Situ* and Real-Time Surface-Enhanced Infrared Study of Electrochemical Reaction. *Appl. Spectrosc.* **1997**, *51*, 512–518.
54. Schreiber, F. Structure and Growth of Self-Assembled Monolayers. *Prog. Surf. Sci.* **2000**, *65*, 151–256.
55. Hölzle, M. H.; Wandlowski, Th.; Kolb, D. M. Phase Transition in Uracil Adlayers on Electrochemically Prepared Island-free Au(100)−(1×1). *J. Electroanal. Chem.* **1995**, *394*, 271–275.
56. Gao, P.; Gosztola, D.; Weaver, M. J. Surface-Enhanced Raman-Spectroscopy as a Probe of Electro-organic Reaction Pathways. 1. Processes Involving Adsorbed Nitrobenzene, Azobenzene, and Related Species. *J. Phys. Chem.* **1988**, *92*, 7122–7130.
57. Frens., G. Controlled Nucleation for The Regulation of the Particle Size in Monodisperse Gold Suspensions. *Nat. Phys. Sci.* **1973**, *241*, 20–22.
58. Liz-Marzan, L. M.; Giersig, M.; Mulvaney, P. Synthesis of Nanosized Gold-Silica Core−Shell Particles. *Langmuir* **1996**, *12*, 4329–4335.
59. Lu, Y.; Yin, Y. D.; Li, Z. Y.; Xia, Y. A. Synthesis and Self-Assembly of Au@$SiO_2$ Core−Shell Colloids. *Nano Lett.* **2002**, *2*, 785–788.